

Teleoperator Coupling Dynamics Impact Human Motor Control Across Pursuit Tracking Speeds

Jacob D. Carducci ¹, Member, IEEE, Noah J. Cowan ², Fellow, IEEE,
and Jeremy D. Brown ³, Senior Member, IEEE

Abstract—Robotic teleoperators introduce novel electromechanical dynamics between the user and the environment. While considerable effort has focused on minimizing these dynamics, we lack a robust understanding of their impact on user task performance across the range of human motor control ability. Here, we utilize a 1-DoF teleoperator testbed with interchangeable mechanical and electromechanical couplings between the leader and follower to investigate to what extent, if any, the dynamics of the teleoperator influence performance in a visual-motor pursuit tracking task. We recruited $N = 30$ participants to perform the task at frequencies ranging from 0.55–2.35 Hz, with the testbed configured into Mechanical, Unilateral, and Bilateral configurations. Results demonstrate that tracking performance at the follower was similar across configurations. However, participants’ adjustment at the leader differed between Mechanical, Unilateral, and Bilateral configurations. In addition, participants applied different grip forces between the Mechanical and Unilateral configurations. Finally, participants’ ability to compensate for coupling dynamics diminished significantly as execution speed increased. Overall, these findings support the argument that humans are capable of incorporating teleoperator dynamics into their motor control scheme and producing compensatory control strategies to account for these dynamics; however, this compensation is significantly affected by the leader-follower coupling dynamics and the speed of task execution.

Index Terms—Compensation, dynamics, telerobotics, teleoperation, tracking, transparency.

I. INTRODUCTION

TELEOPERATORS allow humans to sense and manipulate remote environments separated by distance or scale, often

Received 20 December 2023; revised 25 June 2024, 6 December 2024, and 21 February 2025; accepted 23 February 2025. Date of publication 27 February 2025; date of current version 21 March 2025. This work was supported by National Science Foundation under Grant #1910939. This article was recommended for publication by Associate Editor M. Zhu and Editor-in-Chief D. Prattichizzo upon evaluation of the reviewers’ comments. (Corresponding author: Jacob D. Carducci.)

This work involved human subjects or animals in its research. Approval of all ethical and experimental procedures and protocols was granted by the Johns Hopkins School of Medicine Institutional Review Board under Application No. IRB00263386, and performed in line with the Declaration of Helsinki.

Jacob D. Carducci was with the Department of Mechanical Engineering, Johns Hopkins University, Baltimore, MD 21218 USA. He is now with the Department of Rehabilitation Science, Emory University, Atlanta, GA 30322 USA (e-mail: jdcardu@emory.edu).

Noah J. Cowan and Jeremy D. Brown are with the Department of Mechanical Engineering, Johns Hopkins University, Baltimore, MD 21218 USA (e-mail: ncowan@jhu.edu; jdelainebrown@jhu.edu).

This article has supplementary downloadable material available at <https://doi.org/10.1109/TOH.2025.3546522>, provided by the authors.

Digital Object Identifier 10.1109/TOH.2025.3546522

1939-1412 © 2025 IEEE. All rights reserved, including rights for text and data mining, and training of artificial intelligence and similar technologies. Personal use is permitted, but republication/redistribution requires IEEE permission. See <https://www.ieee.org/publications/rights/index.html> for more information.

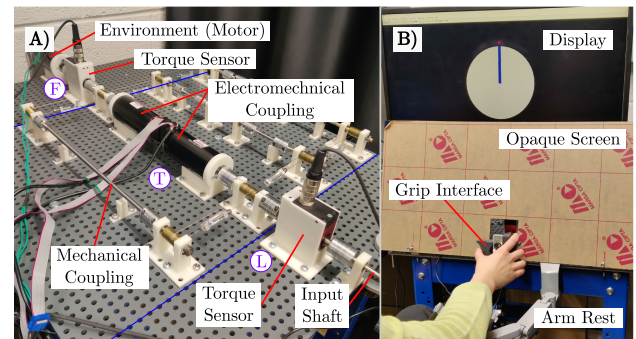


Fig. 1. Experimental testbed and setup. (a) Teleoperator testbed with reconfigurable couplings (circled T) between the leader side (circled L) and the follower side (circled F) (see [11] for complete details). A steel rod creates a rigid mechanical coupling for the Mechanical teleoperator configuration, whereas two DC motors (Maxon RE50) create an electromechanical coupling for the Unilateral and Bilateral teleoperator configurations. The elastic and damping transmissions in the background were decoupled and unused in this experiment. The leader side of the testbed connects to a grip interface (not pictured), while the follower side connects to a DC motor (Maxon RE50), rendering a virtual environment. Torque sensors measure the input and output torque on the leader and follower sides, respectively. (b) A user controls the grip interface with their wrist during the pursuit tracking task (displayed on the monitor), while visual feedback of the testbed is occluded by an opaque screen.

when direct manipulation is not viable, safe, or preferred [1], [2]. Teleoperators are found in many fields including medicine [3], [4], extreme environments [5], [6], and hazardous material handling [7], [8]. A more comprehensive overview of teleoperators is described in [1]. The ideal teleoperator intuitively maps human input to end-effector output through a direct coupling between the leader and follower side of the device. In a similar fashion, ideal teleoperators accurately reflect environmental feedback to the human operator through the same leader-follower coupling. The original teleoperators developed by Goertz attempted to achieve this ideal through a direct mechanical coupling and a kinematically-identical leader and follower [9], [10].

Unlike Goertz’s mechanical teleoperators, modern bilateral force-reflecting teleoperators typically employ electromechanical couplings between the leader and follower, which introduce unwanted closed-loop dynamics that impact the accuracy of leader-follower tracking and the quality of force feedback [12]. These dynamics can also destabilize the control loop due to sensor quantization, sample and hold effects, and communication latency, which lead to energy leaks into the system [1], [13], [14]. While closed-loop controllers can be designed to

dissipate such energy injections, these approaches degrade the overall transparency of the teleoperator [15]. Therefore, while it is theoretically possible to ensure perfect impedance reflection and kinematic correspondence in an electromechanically coupled teleoperator, these systems are practically unattainable in real-world implementations.

Given the practical reality of non-transparent teleoperation, it is worth questioning to what extent humans can compensate for the unwanted closed-loop dynamics introduced through electromechanical control schemes. In human motor control, it has been observed that humans use sensory information to compensate for and incorporate the dynamics of tools during use [16], [17], [18]. Based on a given set of kinematic goals, humans are capable of learning from environmental interaction to update their subjective experience and adapt their motor strategies [19]. Specifically, the central nervous system (CNS) generates a compensatory inverse model of the environment [20] to cancel out nonlinear dynamics [21]. The CNS then modifies the impedance of the arm from muscle co-activation to restabilize the interaction and updates the inverse model from sensory mismatch to improve robustness [22], [23].

For teleoperation in particular, our understanding of these compensation and adaptation strategies is relatively nascent. Previous research from our lab and others has suggested that teleoperator dynamics do affect users' motor control strategy [24], [25].

While insightful, these prior investigations have either focused on a narrow range of human motor control bandwidth, a narrow range of teleoperation transmission couplings (e.g., unilateral), or have only focused on time-domain measures of task performance. Thus, we lack a comprehensive and fundamental understanding of the manner in which human motor control through a teleoperator varies as a function of both the teleoperator's transmission dynamics and the human operator's inherent motor controllability [26], [27]. More specifically, it is unclear to what extent different teleoperator transmission couplings (e.g., direct mechanical, unilateral, bilateral) impact the human operator's ability to accurately control the teleoperator's leader-follower behavior both temporally and spatially across a wide range of task execution frequencies.

In this study, we address this gap in knowledge by investigating human users' ability to perform a pursuit tracking task through a variable transmission teleoperator across a wide bandwidth of operation frequencies.

Utilizing a previously developed teleoperator testbed with independent mechanical and electromechanical couplings between leader and follower [11], [25], we examine to what extent users can accurately perform a visual-motor pursuit tracking task of a predictable sinusoidal signal at various frequencies across the range of human capabilities [26], [27]. We specifically focus on exploration at the wrist (pronation/supination) given its important role in human motion correction during upper-limb tasks [28]. In addition, we chose a one-degree-of-freedom (DoF) tracking task of predictable signals to better measure and understand any performance changes before generalizing to higher-DoF tasks with unpredictable signals, which can become more complicated due to motor control synergies on the user side

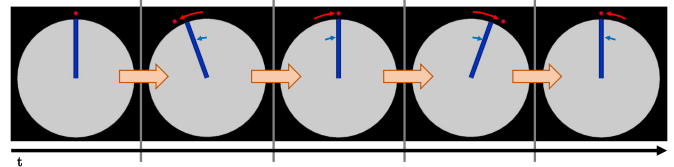


Fig. 2. Tracking task progression. An example display of periodic object-tracking over time. As the ball followed a path indicated by the red arrow, the participant attempted to match the position of the ball by actively aligning a pointer, as indicated by the blue arrow. The visco-elastic disk is the gray circle in the background.

and kinematic constraints on the teleoperator side. During this tracking task, we also record the user's interaction grip force, as arm flexor activation has been shown to be a proxy for arm impedance [29], [30].

Overall, we hypothesize that 1) teleoperator compensation breaks down when the frequency of sinusoidal pursuit tracking is too high, 2) the extent of compensation differs between distinct transmission configurations with unique dynamics, and 3) the user modulates their limb impedance to adjust their control strategy when compensating for different transmission dynamics. In what follows, we introduce our experimental apparatus, experimental protocol, and experimental findings, followed by a discussion of the broader implications of this work in the field of teleoperation.

II. METHODS

A. Participants

$N = 30$ individuals (10 female, 20 male, age = 24.8 ± 7.49) were recruited to participate in the pursuit tracking experiment. All participants were affiliated with Johns Hopkins University or Johns Hopkins Hospital. 25 participants self-reported as being right-hand dominant, three self-reported as ambidextrous with a right-hand preference, and two self-reported as ambidextrous with a left-hand preference. All participants performed the experiment with their right hand regardless of hand dominance. All participants provided written informed consent according to a protocol approved by the Johns Hopkins School of Medicine Institutional Review Board (Study# IRB00263386). Participants were compensated at \$10/hour.

B. Pursuit Tracking Task

Participants utilized the teleoperator testbed (see Section II-C) to perform a pursuit tracking task. In the task, participants controlled the angle of a virtual rotational pointer (blue rectangle in Fig. 2) that represented the follower output of the teleoperator by pronating/supinating their wrist on the leader input of the teleoperator. The virtual pointer was affixed to a massless virtual disk object (grey circle in Fig. 2), which was rendered as having the visco-elastic dynamics of a virtual torsional spring of $1.25 \times 10^{-3} \text{ N} \cdot \text{m}/^\circ$ ($7.16 \times 10^{-2} \text{ N} \cdot \text{m}/\text{rad}$) and a virtual dampener of $5.00 \times 10^{-5} \text{ N} \cdot \text{m} \cdot \text{s}/^\circ$ ($2.86 \times 10^{-3} \text{ N} \cdot \text{m} \cdot \text{s}/\text{rad}$). These virtual environment dynamics were designed to emulate a real physical environment with visco-elastic dynamics that were

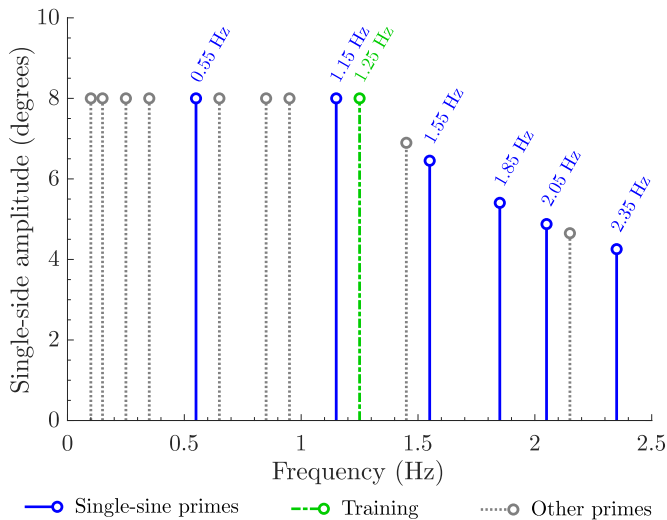


Fig. 3. Visualization of sinusoidal stimulus amplitudes used for pursuit tracking. All stimulus frequencies were prime multiples of the fundamental frequency (0.05 Hz). Similar to [32], amplitudes were constant for frequencies up to and including 1.15 Hz, and above this frequency, amplitudes were scaled inversely proportional to frequency, maintaining a constant peak velocity. A subset of frequency-amplitude pairs were selected for single-sine tracking, emphasized in blue.

separate from the teleoperator dynamics. Although the inertia of the virtual disk was not rendered, the real inertia of the DC motor rendering the virtual disk was perceptible.

The goal of the task was to control the virtual pointer through the teleoperator to track a virtual ball whose rotational movement was governed by single-sine and sum-of-sine waveforms of varying frequency (see Fig. 2). The frequencies of the sine waves were determined using a methodology adapted from Zimmet et al. in which frequencies are generated as prime multiples of a fundamental frequency [31]. With a fundamental frequency of 0.05 Hz, 15 prime multiples were generated up to 2.35 Hz.

Based on interesting spatial and temporal performance differences we observed during pilot testing, we subsequently down-selected from 15 frequencies to the following six frequencies for the single-sine tracking frequencies: 0.55 Hz, 1.15 Hz, 1.55 Hz, 1.85 Hz, 2.05 Hz, and 2.35 Hz. 1.25 Hz was selected as a separate training frequency, also based on pilot results. Amplitudes for these single-sine periodic signals were determined using a piecewise plateau-inverse-law function of frequency. More specifically, lower frequencies below the training frequency shared the same periodic amplitude, while frequencies above 1.25 Hz had amplitudes proportional to the inverse of their frequency. This frequency law is illustrated in Fig. 3. This choice was made so participants could track at constant rotational velocity and, therefore, prevented participants from having to track large displacements at high frequencies and arc velocities.

The final waveform was a sum-of-sines trajectory generated from adding single-sine waves of all 15 prime multiples of 0.05 Hz up to 2.35 Hz, with amplitudes obeying the piecewise law in Fig. 3. The purpose of the sum-of-sines task was to set a baseline for unpredictable movement and to act as a catch trial. This exploration of predictable and unpredictable targets

is a standard practice in tracking research [25], [31], [33], [34] to investigate the generalizability of control and demonstrate ecological validity.

C. Teleoperation Testbed

The teleoperation testbed is an experimental apparatus that models a single-DoF teleoperator with modular couplings between leader and follower, shown in Fig. 1. While key features of the testbed relevant to this study are explained below, complete details of the mechatronic design can be found in [11]. In addition, a preliminary study of human tracking using the testbed can be found in [25].

The testbed can be reconfigured into a mechanical teleoperator or an electromechanical (EM) teleoperator with unilateral or bilateral modes. The testbed consists of four subsystems: 1) operator interface, 2) reconfigurable leader/follower coupling, 3) environment, and 4) data acquisition and control. Notably, this design allows the testbed to be configured into different teleoperator architectures while preserving the same user input and environmental output.

1) *Operator Input*: The operator input is equipped with a grip interface made from 3D-printed grips mounted to either side of a 10 kg rated beam load cell (Transducer Techniques LSP-10) to capture grip force. The entire user input interface is connected to the teleoperator leader through a 316 stainless steel shaft.

2) *Reconfigurable Leader/Follower Coupling*: The input shaft (316 stainless steel) on the teleoperator leader connects to a Futek TRS600 (5 N-m) torque sensor and then to Maxon RE50 (200 W) motor equipped with a 500 CPT HEDL encoder. Likewise, the output shaft on the teleoperator follower connects to a Maxon RE50 (200 W) motor equipped with a 500 CPT HEDL encoder and a Futek TRS600 (5 N-m) torque sensor before connecting to the environment. Between the leader and follower, multiple transmission shafts can be selectively coupled or uncoupled (using screw-type shaft couplings) to create distinct mechanical and electromechanical teleoperator architectures. Capstan drives are used to transmit energy through each of the transmissions from leader to follower (and vice versa). For this study, the following three teleoperator transmission configurations were used:

a) *Mechanical*: The Mechanical teleoperator utilizes a mechanical transmission to couple leader and follower that consist of a 316 stainless steel rod directly coupled to each side without any torque or position scaling. This bilateral configuration inherently provides kinematic correspondence and force reflection. The leader and follower motors are mechanically connected but not energized for this configuration.

b) *Unilateral (EM)*: The Unilateral teleoperator configuration utilizes an electromechanical transmission to couple the leader and follower. In this configuration, the position of the follower motor tracks the position of the leader motor in a position-control scheme; however, no feedback torque is rendered on the leader motor. The rigid mechanical rod is decoupled for this configuration.

c) *Bilateral (EM)*: The Bilateral teleoperator configuration utilizes an electromechanical transmission to couple leader and

TABLE I
TRANSFER FUNCTIONS (FROM TORQUE (mNm) TO POSITION (DEGREES)) IN
DIFFERENT VIRTUAL ENVIRONMENTS ACROSS ALL TELEOPERATOR
TRANSMISSION MODES

	Free-space	Visco-elastic disk
Mechanical	$\frac{271.26}{s^2+0.02s+0.08}$	$\frac{528.32}{s^2+14.61s+586.28}$
Unilateral	$\frac{1077.0}{s^2+0.00s+0.74}$	$\frac{890.24}{s^2+0.00s+0.08}$
Bilateral	$\frac{234.68}{s^2+0.26s+0.00}$	$\frac{667.77}{s^2+15.80s+592.02}$

follower. In this configuration, the position of the follower motor tracks the position of the leader motor, and the position of the leader motor tracks the position of the follower motor in a position-position control scheme. The rigid mechanical rod is decoupled for this configuration.

3) *Virtual Environment*: The output shaft on the teleoperator follower connects to the environment, which consists of a Maxon RE50 (200 W) motor equipped with a 500 CPT HEDL encoder. The motor can render virtual environments with a 4.67×10^{-1} N·m peak torque and 2.33×10^{-1} N·m continuous torque. This motor was used to generate the virtual visco-elastic disk connected to the follower end of the teleoperator.

4) *Data Acquisition and Control*: All Maxon motors are current-controlled with a Quansar AMPAQ L4 amplifier, which receives commands from a Quansar QPiDe DAQ operating at 1 kHz from Simulink 10.2 in MATLAB 2020b (Mathworks; Natick, MA, USA) with QUARC 2020 SP2 (Quanser Software; Markham, ON, CA) on a Dell Precision T4810 Workstation. To generate the electromechanical transmission for the Bilateral configuration, the following proportional-derivative (PD) control law was utilized:

$$\tau_f = k_p(\theta_l - \theta_f) + k_d(\dot{\theta}_l - \dot{\theta}_f) \quad (1)$$

$$\tau_l = k_p(\theta_f - \theta_l) + k_d(\dot{\theta}_f - \dot{\theta}_l) \quad (2)$$

where τ_l and τ_f are the torques commanded to leader and follower motors in N·m, θ_l and θ_f are the encoder angles from the leader and follower motors in radians, $k_p = 2.68 \times 10^{-1}$ N·m/rad is the proportional gain, and $k_d = 2.68 \times 10^{-2}$ N·m·s/rad is the derivative gain. These coupling gains were determined through pilot testing in a previous study [25] to be the best balance of transparency and stability. For the Unilateral teleoperator, the same PD control law was utilized, except the leader motor did not output torque ($\tau_l = 0$).

D. Teleoperator Testbed Dynamics

Transfer functions for each teleoperator configuration mode at the leader interface are listed in Table I. The transfer functions were characterized for two different virtual environments, rendered using the environment motor: (1) a free-space environment with the environment motor de-energized, and (2) the visco-elastic disk environment used in the experiment. These transfer functions were obtained by driving the leader to follow a desired chirp signal that oscillated between ± 90 degrees relative to the initial position at the chirp start (physically set as the midpoint between rotational limits of the teleoperator).

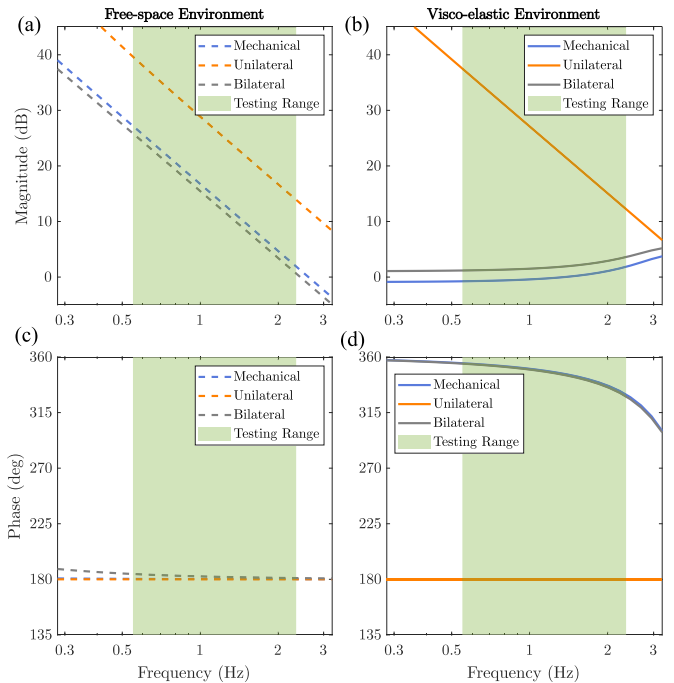


Fig. 4. Frequency response fits for teleoperator transmission system identification. Bode plots showing magnitude (A & B) and phase (C & D) spectrums of the frequency responses from the teleoperator interfacing with free-space (A & C) and with a virtual visco-elastic disk object (B & D). Different configuration modes are indicated by thick colored lines. The prime frequencies in the green-shaded region indicate the frequencies used in the experiment. The input motor torque (mNm) acts as input, and the leader shaft rotation (degrees) acts as output.

The chirp frequency increased linearly from 0.05 to 3.0 Hz over 30 seconds, covering the general bandwidth of human motion expected during the pursuit tracking task [26], [31], [32]. The chirp signal was repeated twice for each combination of teleoperator configuration (Mechanical, Bilateral, and Unilateral) and environment (Free-space and Visco-elastic disk). Second-order system models (with applied shaft torque as input and leader shaft displacement as output) were estimated with the MATLAB 2021a System Identification Toolbox using the `tfest` command. Before linear fit estimation, the torque and displacement signals had frictional features isolated and removed, and both signals had sensor noise filtered out with a Butterworth filter at 6 Hz half-power cutoff frequency. The filter was applied forwards and backwards as a zero-phase digital filter using the `filtfilt` command. Complete details of the signal conditioning and transfer function fitting are included in the Supplemental Section. Corresponding Bode plots of the resulting frequency response functions are shown in Fig. 4.

E. Study Design

Upon confirmation of written informed consent, participants were seated in front of the testbed, and the seat and forearm rest were height-adjusted until the arm was comfortable and approximately co-linear with the input shaft. Regardless of self-reported handedness, all participants used their right hand and wrist to interact with the testbed. An opaque screen was

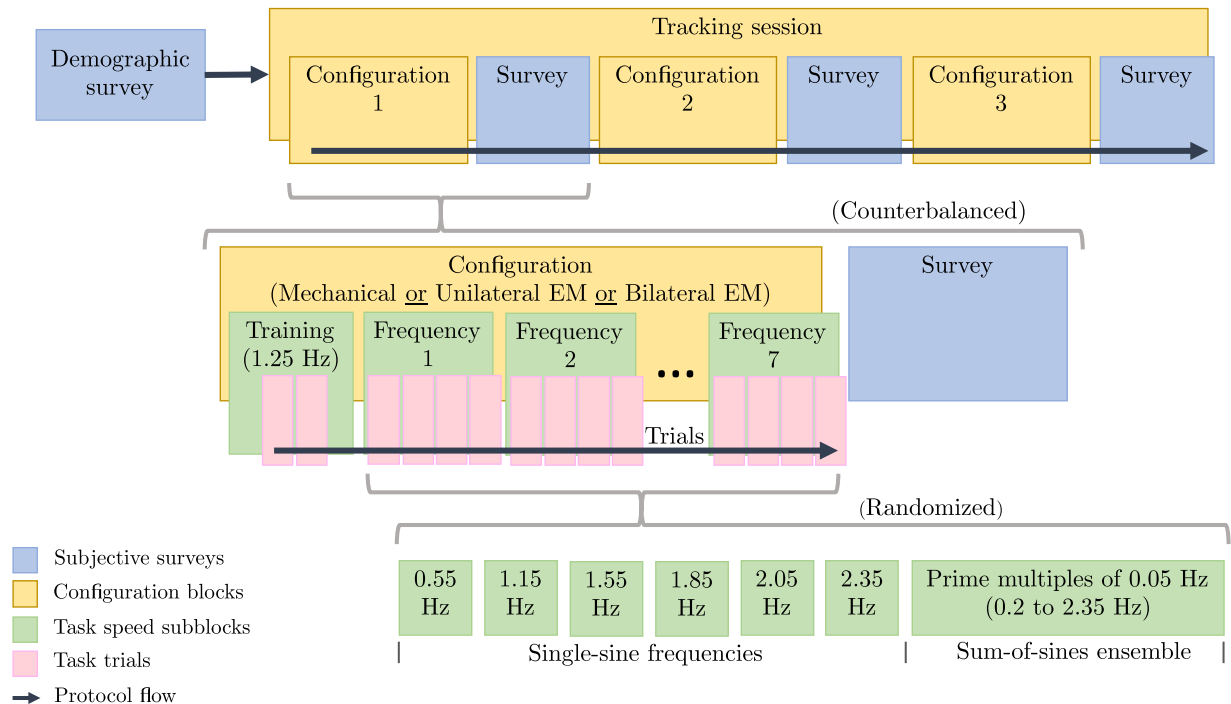


Fig. 5. Experimental protocol illustration. The protocol progression of the tracking experiment for a typical participant session. Note that training frequencies lasted only two trials, whereas other task frequency subblocks lasted four trials.

fastened to the front of the testbed, shown in Fig. 1(b), to ensure the participant did not get visual rotational cues from the transmission mechanics. A high-definition monitor was placed above the opaque screen to provide instructional cues and visual feedback. In addition, noise-cancelling headphones were fitted to the participant's ears to mitigate audio cues.

The study utilized a within-subjects design in which each participant performed the pursuit tracking task with all three teleoperator transmission configurations. The testing session for each participant was divided into three blocks into which the three transmission configurations were counterbalanced. Each configuration block consisted of 30 trials, with the first two trials always containing the training frequency (1.25 Hz, based on pilot testing). The remaining 28 trials consisted of four trials of each of the seven tracking frequencies (six single-sine and one sum-of-sine), with the frequency presentation order pseudo-randomized and counterbalanced across participants. The number of training and tracking trials was determined from pilot testing and guidance from prior investigations with the testbed [25] in an effort to balance statistical power and participant retention. After all 30 trials for a given configuration block, the participant took a survey followed by a 3-minute-minimum break before starting the next configuration block. A graphical summary of a typical study session is depicted in Fig. 5.

During each trial, the participant pinched onto a grip interface to operate the teleoperator, shown in Fig. 1(b). Participants oriented their hands such that at least one finger was in contact with the 3D-printed contact on each side, and their fingers were not contacting the interior load cell. In this way, participants interacted with the teleoperator by squeezing and rotating only

the designated plastic contacts of the grip interface. During each trial, participants were instructed to pronate and supinate their wrists to control the pivot of the virtual rotational pointer using the grip interface.

Each trial began with an auditory cue stating "Start". When a virtual ball object started orbiting the disk perimeter independently, the participant had to align the pointer to the ball as well as they could throughout the task duration.

The target ball always started at zero position above the disk, ramped up to a full oscillation centered around zero position after 5 seconds, and continued full oscillation for 20 seconds at one of the predetermined frequencies discussed in Section II-B.

The participant repeated the tracking task for all configuration blocks until session conclusion or a request for early study termination. Early termination of the session occurred if the participant expressed significant discomfort or the investigator deemed it unsafe for the participant to continue in the study.

F. Survey

Before the first experimental block, each participant completed a demographic survey with questions regarding age, gender, and handedness. After each experimental block, participants completed the following questionnaire on a scale of 1-6 (Strongly Disagree to Strongly Agree):

- 1) The task was easy to perform.
- 2) I was able to accurately track the moving ball.
- 3) My tracking accuracy improved with time.
- 4) My tracking accuracy was worse during tasks that seemed fast.

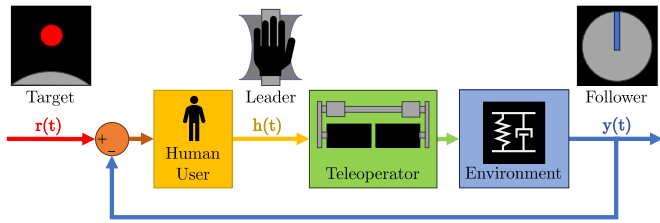


Fig. 6. Human-teleoperator closed-loop feedback model. A simplified closed human-in-the-loop control system where the human user controls a leader input $h(t)$, attempting to rotationally align an output pointer $y(t)$ to a reference target ball $r(t)$ through a teleoperator.

- 5) My tracking accuracy was better during tasks that seemed slow.
- 6) I relied on visual feedback for ball tracking.
- 7) I relied on haptic feedback for ball tracking.
- 8) I was in control of the disk/stick.
- 9) The motion of the disc/stick was unpredictable.

Furthermore, participants were allowed to voluntarily share general comments at the conclusion of the session.

G. Task Performance Metrics

The following data analysis methodology has been adapted from [31], [35] and utilizes a frequency-domain approach to analyze task performance. This frequency-domain approach is built on the fact that our teleoperator testbed and the human operators can be modeled as a human-in-the-loop closed-loop dynamical system, as illustrated in Fig. 6.

For each pursuit tracking task, our system tracks time-series rotational positions from the leader encoder $h(t)$, follower encoder $y(t)$, and virtual ball $r(t)$. During analysis of each task, these three position signals are the signals of interest. These time-series signals are shown in Fig. 7(a) for a representative training trial. Each vector of time-series rotational positions is converted into a single-sided spectrum of frequency components via a fast Fourier transform (FFT) implementation of the discrete Fourier transform (DFT) in MATLAB 2021a (Mathworks; Natick, MA, USA). Complex-valued FFTs for the leader signal, follower signal, and virtual target are $H(f)$, $Y(f)$, and $R(f)$, respectively. The resulting spectral output from time-to-frequency conversion for the training trial is shown in Fig. 7(c). After frequency-domain conversion, both leader and follower responses were compared to the target at task-specific frequencies, resulting in ratios of complex phasors for the leader $TF_L(f) = H(f)/R(f)$ and for the follower $TF_Y(f) = Y(f)/R(f)$. From these phasor ratios, profiles of gain (phasor magnitude) and phase (phasor angle) can be computed. Relative gains and phases act as tracking performance metrics to determine how well the teleoperator leader/follower positions tracked the target. For phasor magnitude, perfect tracking corresponds to a gain ratio of 1, with ratios > 1 corresponding to leader/follower overshoot and ratios < 1 corresponding to undershoot with respect to the target. For phasor angle, perfect tracking corresponds to a phase difference of 0, with differences < 0 indicating leader/follower lag and higher differences > 0 indicating leader/follower lead

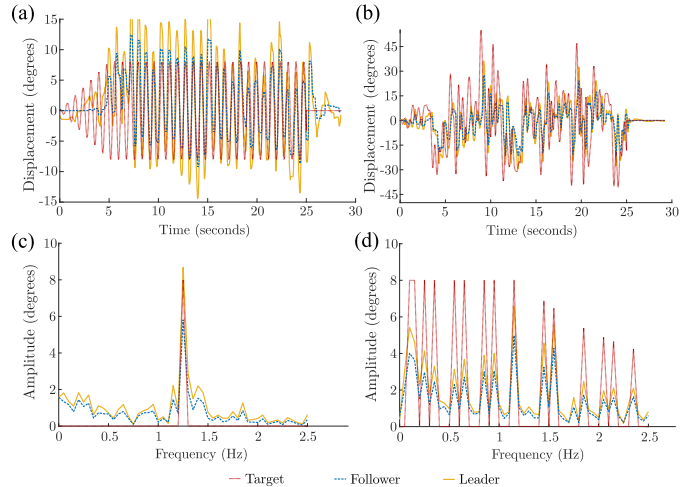


Fig. 7. Representative time-domain and frequency-domain tracking signals. (a) Rotational trajectories of the virtual target $r(t)$ (red-dotted), follower output $y(t)$ (blue-dashed), and leader input $h(t)$ (yellow-solid) from a representative training trial. Note that the target exhibited transient ramping at trial start for 5 seconds and maintained constant oscillation for another 20 seconds. (b) Rotational trajectories from a representative sum-of-sines task. (c) Amplitude spectrums in frequency-domain from FFT decompositions applied to time-series rotational trajectories of the virtual target $R(f)$, environment-connected follower shaft $Y(f)$, and participant-controlled leader shaft $H(f)$ from the same representative training trial as in (a). (d) Amplitude spectrums obtained from time-series rotational trajectories of the sum-of-sines task in (b).

with respect to the target. Taken together, these metrics measure the spatial and temporal adjustments of the user on the leader side of the teleoperator to track the target with the follower side of the teleoperator.

In addition to tracking performance, we also measured grip force on the user input. Forces from the grip interface sensor were reported in Newtons, averaged at task frequencies across participants, and clustered by teleoperator configuration.

H. Statistical Analysis

Linear mixed-effects (LME) models were fitted to performance measures of gain ratios, phase ratios, and grip forces. For each measure, we ran separate LME models for each factor, controlling for random effects. Specifically for each model, one independent measure is set as the main effect (e.g., teleoperator configuration), and the other factors are set as random effects (e.g., trials and frequency). With 5 dependent measures and 3 independent factors, we had a total of 15 separate LME models fitted. The performance measures were then compared pairwise using general linear hypothesis testing (GLHT) to reveal two-sided significant differences between teleoperator configurations, target frequencies, and trial repetitions.

When needed, tests for normality and for homogeneity of variance were conducted. Due to multiple comparisons, post-hoc Tukey corrections were applied. RStudio 2022.02.3 Build 492 (Posit Software; Boston, MA) with the `lmer4_1.1-35.5`, `lmerTest_3.1-3`, and `multcomp_1.4-26` packages were used for all analyses.

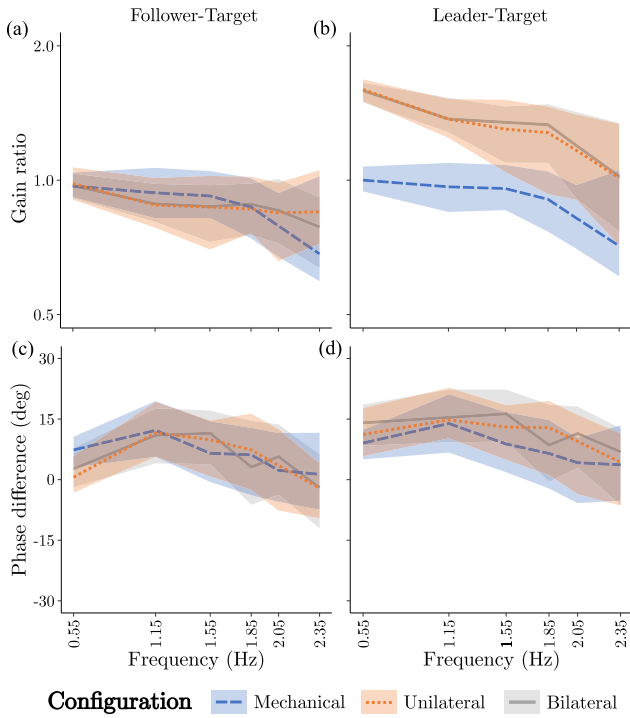


Fig. 8. Frequency-domain responses during human tracking. Ribbon-style interpolated Bode plots of the median (solid line) and interquartile range (shaded area) across all single-sine task frequencies for (a) follower-target gain ratio, (b) leader-target gain ratio, (c) follower-target phase difference, and (d) leader-target phase difference. Phasor metrics were aggregated across participants and trials, and teleoperator configurations are indicated by color.

To determine any significant differences in survey responses between configuration modes, a one-way within-subjects ANOVA test was conducted for all nine survey questions. If any significant differences were found, multiple comparison t-tests would be conducted with post-hoc Tukey corrections.

Given that there were two participants with a left-hand preference, we conducted a sensitivity analysis, in which we reran all statistical analyses with these two participants excluded. Overall, the findings changed very little from those of the $N = 30$ results presented below. Still, we have included these results in the Supplemental Section for a full review.

III. RESULTS

All performance measure samples passed Shapiro tests for normality and passed Bartlett's tests for homogeneity of variance. Therefore, we conducted statistical analysis with parametric testing. A graphical summary of frequency-domain metrics from each transfer function response is shown in Fig. 8. From this figure, we observe differences in tracking performance that are discussed further in the following sections.

A. Follower Tracking Performance is Similar Across Teleoperator Configurations

We found a significant main effect of configuration on follower gain (intercept = 0.733, SE = 0.078, $p < 0.001$) but not

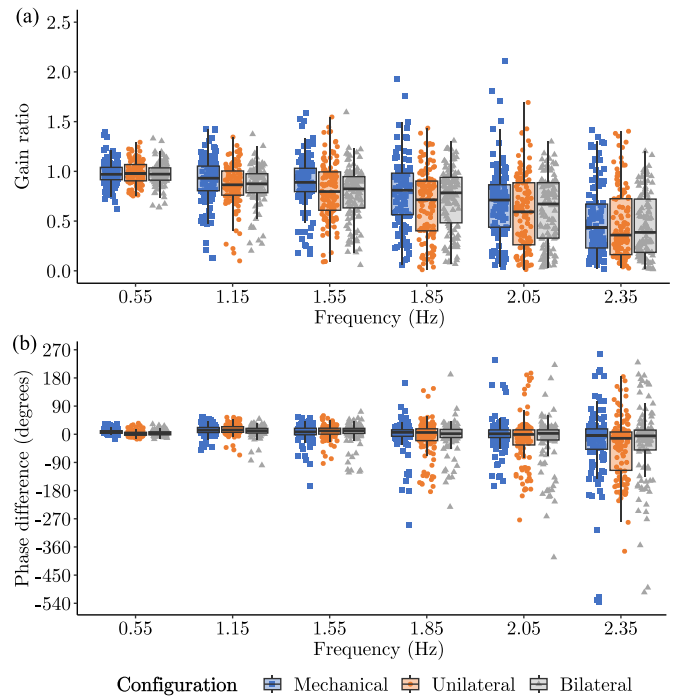


Fig. 9. Follower-target performance by tracking frequency. Gain and phase ratio/difference plots of the follower-target frequency response expressing relative (a) gain ratio and (b) phase difference for all three teleoperator configurations. Ratios and differences are aggregated across participants and trials.

TABLE II
P-VALUES FROM PAIRWISE COMPARISONS OF FOLLOWER-TARGET GAIN RATIOS BETWEEN TRACKING FREQUENCIES

Freq (Hz)	1.15	1.55	1.85	2.05	2.35
0.55	<0.001	<0.001	<0.001	<0.001	<0.001
1.15		0.010	<0.001	<0.001	<0.001
1.55			<0.001	<0.001	<0.001
1.85				<0.001	<0.001
2.05					<0.001

on follower phase (intercept = -4.982 , SE = 8.333, $p > 0.05$). We observed no statistical difference in the follower-target gain ratio ($p > 0.05$ for all pairwise comparisons) between the three teleoperator configurations. We also observed no statistical difference in the follower-target phase difference ($p > 0.05$ for all pairwise comparisons) between the three teleoperator configurations. These results are supported by the visually similar gain and phase ratio/difference plots shown in Fig. 9 between each configuration across all frequencies. These findings demonstrate that teleoperation configuration did not have a significant impact on participants' ability to perform the pursuit tracking task.

B. Tracking Frequency Impacts Follower Performance

We found a significant main effect of frequency on follower gain (intercept = 0.980, SE = 0.035, $p < 0.001$), but not on follower phase (intercept = 4.790, SE = 5.987, $p > 0.05$). We observed several significant differences in the follower-target gain ratio (see Table II) and phase difference (see Table III)

TABLE III
P-VALUES FROM PAIRWISE COMPARISONS OF FOLLOWER-TARGET PHASE DIFFERENCES BETWEEN TRACKING FREQUENCIES

Freq (Hz)	1.15	1.55	1.85	2.05	2.35
0.55	0.319	>0.999	0.043	< 0.001	< 0.001
1.15		0.520	< 0.001	< 0.001	< 0.001
1.55			0.016	< 0.001	< 0.001
1.85				0.773	< 0.001
2.05					< 0.001

TABLE IV
P-VALUES FROM PAIRWISE COMPARISONS OF LEADER-TARGET GAIN RATIOS BETWEEN TRACKING FREQUENCIES

Freq (Hz)	1.15	1.55	1.85	2.05	2.35
0.55	< 0.001				
1.15		0.002	< 0.001	< 0.001	< 0.001
1.55			< 0.001	< 0.001	< 0.001
1.85				< 0.001	< 0.001
2.05					< 0.001

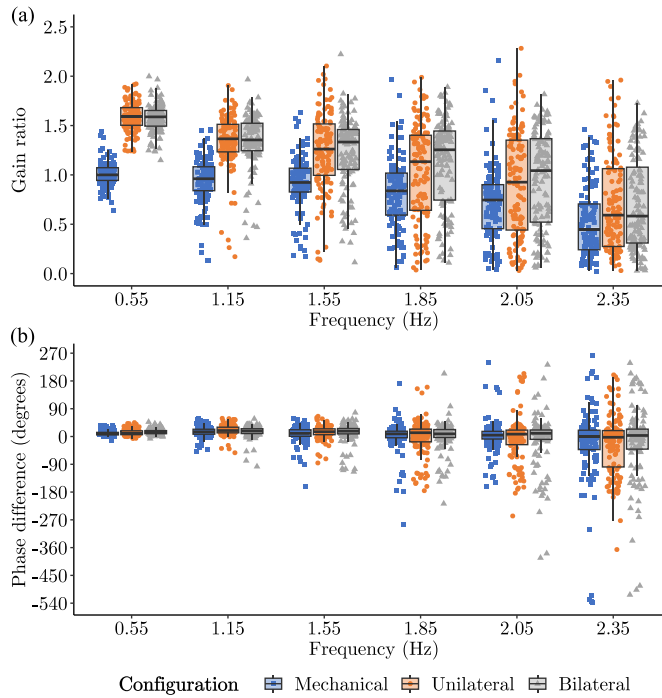


Fig. 10. Leader-target adjustment by tracking frequency. Gain and phase ratio/difference plots of the leader-target frequency response expressing relative (a) gain ratio and (b) phase difference for all three teleoperator configurations. Ratios and differences are aggregated across participants and trials.

between task frequencies. These findings are irrespective of the teleoperator configuration used and demonstrate that participants' tracking performance accuracy decreased both spatially and temporally as task frequency increased.

C. Leader Tracking Adjustment Differs Between Teleoperator Configurations

We found a significant main effect of teleoperator configuration on leader gain (intercept = 1.156, SE = 0.110, $p < 0.001$), but not on leader phase (intercept = 2.278, SE = 8.541, $p > 0.05$). We found a significantly different gain ratio between the Mechanical and Bilateral configurations ($p < 0.001$) and between the Mechanical and Unilateral configurations ($p < 0.001$) (see Fig. 10(a)). We found no statistical difference in the leader-target phase difference ($p > 0.05$ for all pairwise comparisons) between the three teleoperator configurations (see Fig. 10(b)). These configuration-dependent findings are irrespective of the frequency of exploration. Together, these

TABLE V
P-VALUES FROM PAIRWISE COMPARISONS OF LEADER-TARGET PHASE DIFFERENCES BETWEEN TRACKING FREQUENCIES

Freq (Hz)	1.15	1.55	1.85	2.05	2.35
0.55	0.910	0.990	0.006	< 0.001	< 0.001
1.15		0.571	< 0.001	< 0.001	< 0.001
1.55			0.044	< 0.001	< 0.001
1.85				0.792	< 0.001
2.05					< 0.001

findings highlight how participants had to make significantly different spatial adjustments, but not significantly different temporal adjustments, on the leader input of the teleoperator to achieve tracking accuracy on the follower output.

D. Tracking Frequency Impacts Leader Adjustment

We found significant main effects of frequency on leader gain (intercept = 1.391, SE = 0.043, $p < 0.001$) and leader phase (intercept = 13.117, SE = 6.254, $p < 0.05$). We observed several significant differences in the leader-target gain ratio (see Table IV) and phase difference (see Table V) across task frequencies. These frequency-dependent findings are irrespective of the teleoperator configuration used and demonstrate that participants' tracking adjustment decreased both spatially and temporally as task frequency increased.

E. Teleoperator Configuration and Tracking Frequency Influence Grip Force

We found significant main effects of configuration on grip force (intercept = 1.689, SE = 0.298, $p < 0.001$) and frequency on grip force (intercept = 1.660, SE = 0.266, $p < 0.001$). There was a significant pairwise difference in grip force between Mechanical and Unilateral configurations ($p = 0.004$). All other comparisons between teleoperator configurations were not significant ($p > 0.05$). Fig. 11 (next page) shows the grip force distributions across all frequencies for the three different teleoperator configurations. Additionally, there were several significant differences in grip force between task frequencies, highlighted in Table VI (next page). Together these findings highlight how the availability of force-reflection in the teleoperator caused the participant to adjust their limb impedance. In addition, these findings demonstrate that changes in limb impedance can occur as a result of tracking frequency.

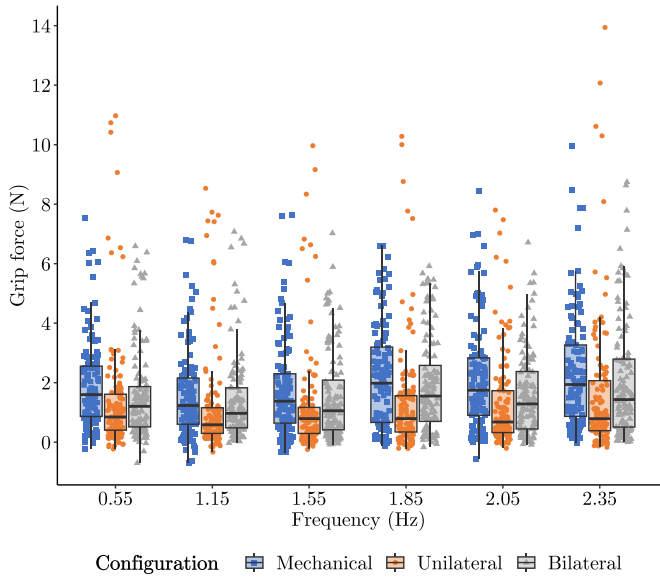


Fig. 11. Grip force by tracking frequency. Box-whisker plots showing the frequency response of participant pinch force for all three teleoperation configurations. Grip forces are aggregated across participants and trials.

TABLE VI
P-VALUES FROM PAIRWISE COMPARISONS OF GRIP FORCE BETWEEN FREQUENCIES

Freq (Hz)	1.15	1.55	1.85	2.05	2.35
0.55	<0.001	0.100	0.048	>0.999	<0.001
1.15		0.538	<0.001	<0.001	<0.001
1.55			<0.001	0.058	<0.001
1.85				0.084	0.034
2.05					<0.001

F. Trial Repetition Impacts Tracking and Grip Force

We found significant main effects of trial repetition on follower gain (intercept = 0.726, SE = 0.077, $p < 0.001$), leader gain (intercept = 1.007, SE = 0.108, $p < 0.001$), and grip force (intercept = 1.803, SE = 0.279, $p < 0.001$). However, we did not find significant main effects of trial repetition on follower phase (intercept = -7.334, SE = 8.168, $p > 0.05$) and leader phase (intercept = -1.044, SE = 8.256, $p > 0.05$). Follower-target gain ratios differed significantly between the first and third trials and between the first and fourth trials ($p = 0.042$ and $p = 0.007$, respectively), irrespective of tracking frequency or teleoperator configuration. Additionally, leader-target gain ratios differed between the first and fourth trials ($p = 0.011$) overall throughout the study. However, no statistical significance was found between trials for follower-target and leader-target phase differences ($p > 0.05$). Furthermore, grip force became significantly different by the third and fourth trial repetitions compared to the first tracking trial ($p = 0.003$ and $p < 0.001$) and between the second and fourth trials ($p = 0.032$) across all tracking frequencies and teleoperator configurations. These findings demonstrate that participants' tracking accuracy decreased with

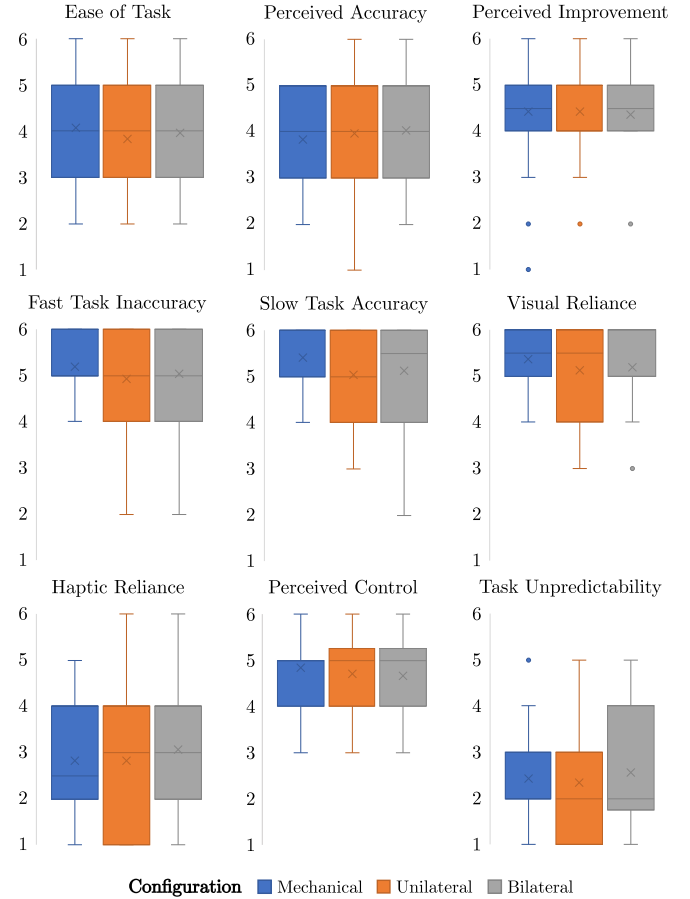


Fig. 12. Task load survey responses. Agreement scores from participants in the post-task survey, scaled from 1 (Strongly Disagree) to 6 (Strongly Agree) and clustered into teleoperator configuration by color. Scores are aggregated across individuals, with the horizontal line in each box indicating the sample medians and vertical x-marks indicating the sample means.

repeated trials and that limb impedance changed with repeated trials.

G. Participants' Subjective Experience Remained Consistent Across Teleoperator Configurations

Box-and-whisker charts of response distributions from the post-configuration surveys are shown in Fig. 12. The one-way ANOVA did not yield any statistically significant differences between configurations in any survey question, indicating that participants did not subjectively experience the teleoperator configurations differently. Meanwhile, higher average scores (>3) in Slow Task Accuracy and Perceived Improvement indicate that participants were perceptive of changes in their motor ability throughout the experiment.

IV. DISCUSSION

In this study, we investigated to what extent the dynamics introduced by different teleoperator transmission couplings impact a user's pursuit tracking task performance across a wide range of task execution speeds. Using a teleoperator testbed that featured interchangeable mechanical, unilateral, and bilateral

transmission configurations, we asked participants to perform a visual-motor pursuit tracking task across a wide range of frequencies within the human motor-control bandwidth. Task performance was evaluated using a frequency-based approach to separately analyze how well both the teleoperator leader and follower tracked the virtual target. We also analyzed participants' grip force to understand to what extent participants attempted to match the impedance of their limb to that of the teleoperator and how this adjustment changed with teleoperator configuration and tracking frequency.

Our utilization of different frequency trajectory profiles was intended to test the limits of human teleoperator control. As the tracking frequency increased, participants' tracking performance in all three teleoperator configurations decreased. The gain ratio error from ideal target tracking at both the teleoperator leader and follower increased as tracking frequencies increased, and the synchronization represented by phase difference worsened at especially higher frequencies above 1.75 Hz. Thus, our first hypothesis is supported, given that task difficulty represented by target frequency impacted performance. These results of performance breakdown over task speed generally agree with hand joystick tracking observations in prior literature [26]. Whereas our original study [25] only tested a composite trajectory of three frequencies from the low end of the bandwidth tested by previous hand joystick tracking [26], our new study investigated performance over a larger bandwidth of task frequencies. This frequency range included frequencies high enough that tracking was subjectively too difficult. These quantitative results are confirmed through higher average scores in Slow Task Accuracy and Fast Task Inaccuracy from participants' subjective responses. Thus, we know that participants had a conscious awareness of their decreasing performance.

While the choice of teleoperator configuration did not have an impact on the follower's tracking performance, we did observe significant differences in tracking adjustment on the leader side. Notably, we found differences in gain ratios between the Mechanical teleoperator and the Unilateral teleoperator and between the Mechanical teleoperator and the Bilateral teleoperator. These differences, however, were not replicated with the phase differences. Overall, this finding supports our second hypothesis, suggesting that participants had to compensate for the teleoperators differently. The Mechanical teleoperator used a mechanical coupling (via a rigid rod) that provided no position or torque scaling nor introduced any unknown dynamics beyond extra inertia and stiffness. On the other hand, the electromechanical transmissions employed by the Unilateral and Bilateral teleoperators introduced delays and varying amounts of position or torque scaling (due to the controller's stiffness and damping) between the operator and the virtual disk. Therefore to accurately perform the tracking task, the operator had to compensate for these dynamics as they rotated the hand fixture. Thus, our results suggest that electromechanical coupling dynamics are harder to compensate for than mechanical coupling dynamics, in particular for spatial accuracy in pursuit tracking.

That we did not find differences in phase tracking from single-sine tasks would separately suggest that participants may have prioritized the temporal demands of tasks over the spatial

demands. This is further supported by the fact that the target single-sine trajectories analyzed were all predictable periodic signals of varying frequency. Together with changed gain performance with more task repetitions, our findings imply that compensation of the teleoperator improved as users became more familiar with the configuration and speed from repeated tracking. Above-average scores in Perceived Improvement from post-configuration responses across all transmissions support this conclusion. It is also worth mentioning here that these results validate those of our original study [25], given that our broader investigation into higher-frequency task execution still included lower frequencies consistent with that study. Extended task execution may have introduced learning effects but may have also caused fatigue or other order effects that counteract. Knowing the specific performance mechanisms from task exposure and familiarity in teleoperative tracking requires further study.

In addition to finding differences in compensatory strategies between our teleoperator configurations, we also observed that our participants used different amounts of grip force when using the Mechanical teleoperator as compared to the Unilateral teleoperator. This finding provides support for our third hypothesis and is consistent with literature demonstrating that humans match their limb impedance to the impedance of their tool [22], [23], including our prior study [25]. Interestingly, we did not find significant differences in grip force between the Mechanical teleoperator and the Bilateral teleoperator, nor between the Bilateral teleoperator and the Unilateral teleoperator. While the Bilateral teleoperator did provide force reflection, the dynamics of the virtual environment did not have the same impact on participants as they did with the Mechanical teleoperator. This may be due to the way in which the dynamics of the electromechanical coupling shaped the effective impedance displayed to participants [12], [13], [24]. Ultimately, this reflected impedance led participants to choose limb impedance values that were not significantly different from both the Mechanical teleoperator and the Unilateral teleoperator. Perhaps the Bilateral teleoperator reflects impedance somewhere in between, but this speculation should be rigorously tested in future studies. The biggest differences in grip force came at the highest task execution frequencies (e.g., 2.35 Hz), which also happens to be where the largest differences in follower tracking performance and leader adjustments were seen. Additionally, the grip force changed with more task repetitions, which further suggests an adaptive user strategy as the dynamics became more familiar to the user.

Our quantitative task performance findings are also substantiated by participants' subjective responses. In particular, participants strongly agreed that they relied on visual cues, which held across all teleoperator configurations. Meanwhile, participants reported slight-to-moderate disagreement that they relied on haptic cues, regardless of configuration. We expected users in a visual-motor task to utilize their vision more, and we found that our participants did not believe they used haptics as much as vision. Both senses can still play a role in incorporating teleoperator dynamics, but tool compensation likely draws heavier from visual information rather than kinesthesia. It is also worth considering that participants may not have completely understood the term "haptic" used in the survey,

which could have caused confusion for some. Still, the difference in responses between sensory modalities (Visual and Haptic) and the consistent response scores between configurations match our observations from surveys in our previous study [25]. Participants also generally agreed that the tool is easy to use and control between transmissions, which may imply that the process of tool incorporation and compensation does not take much physical or cognitive effort. Therefore, the process of incorporating different dynamics was intuitive for participants.

Overall, these results provide a foundational understanding of the manner in which teleoperator dynamics affect the human operator's visual-motor task performance. The knowledge gained from this study can be applied and expanded on in a number of different ways. First, the protocol can be expanded from 1-DoF to 3-DoF tasks. At the wrist alone, there are two other anatomical directions with similar neural control and learning mechanisms, despite different muscle activation patterns. Thus, while users in a 3-DoF wrist teleoperation task should exhibit similar compensation and motor control adaptation in spatial and temporal tracking with different dynamics and speed difficulties, it is still unknown. This is also true for higher-DoF tasks involving the entire arm. Also, the findings from our Unilateral and Bilateral configurations can be compared against those utilizing more advanced teleoperation control laws in multi-DoF task scenarios with predictable and unpredictable task goals. Future studies with novel controllers can utilize the findings we established to measure how well performance improves from operators interacting with these controllers at various task frequencies. Second, while we postulate that users are inverting the plant dynamics of each teleoperator configuration, this theory should actually be tested. Utilizing the approach developed by Yamagami et al. [36], we could utilize the display monitor and motors in the testbed to inject visual and kinesthetic disturbances. This would allow for a more robust estimation of the feedforward-feedback models participants utilize. This approach would allow for comparisons to be made with individuals who have known neurological disorders that limit the formation of feedforward control strategies, such as cerebella ataxia. Finally, future studies should include EMG measures and effective impedance analysis alongside grip force measures to produce more accurate estimations of participants' impedance-matching abilities.

V. CONCLUSION

While teleoperators in the 20th century originally utilized mechanical transmissions to couple leader and follower, current devices rely on electromechanical couplings, which impact device transparency by introducing undesirable closed-loop dynamics. By testing pursuit tracking on a reconfigurable teleoperator testbed, we have demonstrated that users adjust limb effort and behavioral strategy to compensate for different teleoperator dynamics. This compensation, however, breaks down when the task becomes too difficult to track. Overall, we found that the dynamics associated with different couplings do impact tracking performance, especially near the limits of human motor control. Our results provide useful insights into the functional control abilities of users performing visual-motor tasks through a

teleoperator. While these results only focus on pursuit tracking of predictable periodic signals in 1-DoF, our experimental setup and protocol serve as a foundation for future investigations with complex unpredictable signals and novel teleoperator control laws in multi-DoF.

ACKNOWLEDGMENT

The authors would like to thank Dr. Mohit Singhala for providing his expertise on the teleoperator testbed and previous studies. They would also like to thank Di Cao and Yu Yang for their insight on frequency-domain analysis, and the authors would like to thank Ahmed Sabit for statistical consultation on linear mixed-effect models.

REFERENCES

- [1] G. Niemeyer, C. Preusche, S. Stramigioli, and D. Lee, *Telerobotics*, 2nd ed. Cham, Switzerland: Springer, Jul. 2016, pp. 1085–1108.
- [2] T. Sheridan, "Telerobotics," *Automatica*, vol. 25, pp. 487–507, Jul. 1989.
- [3] C. G. Welker, V. L. Chiu, A. S. Voloshina, S. H. Collins, and A. M. Okamura, "Teleoperation of an ankle-foot prosthesis with a wrist exoskeleton," *IEEE Trans. Biomed. Eng.*, vol. 68, no. 5, pp. 1714–1725, May 2021.
- [4] J. Burgner et al., "A telerobotic system for transnasal surgery," *IEEE/ASME Trans. Mechatron.*, vol. 19, no. 3, pp. 996–1006, Jun. 2014.
- [5] O. Khatib et al., "Ocean one: A robotic avatar for oceanic discovery," *IEEE Robot. Automat. Mag.*, vol. 23, no. 4, pp. 20–29, Dec. 2016.
- [6] T. Sheridan, "Space teleoperation through time delay: Review and prognosis," *IEEE Trans. Robot. Automat.*, vol. 9, no. 5, pp. 592–606, Oct. 1993.
- [7] A. Kron, G. Schmidt, B. Petzold, M. Zah, P. Hinterseer, and E. Steinbach, "Disposal of explosive ordnances by use of a bimanual haptic telepresence system," in *Proc. IEEE Int. Conf. Robot. Automat. (ICRA)*, 2004, pp. 1968–1973.
- [8] F. Negrello et al., "Humanoids at work: The WALK-MAN robot in a postearthquake scenario," *IEEE Robot. Automat. Mag.*, vol. 25, no. 3, pp. 8–22, Sep. 2018.
- [9] R. C. Goertz, "Mechanical master-slave manipulator," *Nucleonics*, vol. 12, pp. 45–46, Nov. 1954.
- [10] P. F. Hokayem and M. W. Spong, "Bilateral teleoperation: An historical survey," *Automatica*, vol. 42, pp. 2035–2057, Dec. 2006.
- [11] M. Singhala and J. D. Brown, "A novel testbed for investigating the impact of teleoperator dynamics on perceived environment dynamics," in *Proc. IEEE/RSJ Int. Conf. Intell. Robots Syst.*, Sep. 2021, pp. 8358–8364.
- [12] N. Colonnese and A. M. Okamura, "Analysis of effective impedance transmitted to the operator in position-exchange bilateral teleoperation," in *Proc. IEEE World Haptics Conf. (WHC)*, Jun. 2017, pp. 328–333.
- [13] D. Lawrence, "Stability and transparency in bilateral teleoperation," *IEEE Trans. Robot. Automat.*, vol. 9, no. 5, pp. 624–637, Oct. 1993.
- [14] B. Hannaford and J.-H. Ryu, "Time-domain passivity control of haptic interfaces," *IEEE Trans. Robot. Automat.*, vol. 18, no. 1, pp. 1–10, Feb. 2002.
- [15] J. Artigas, C. Preusche, G. Hirzinger, G. Borghesan, and C. Melchiorri, "Bilateral energy transfer in delayed teleoperation on the time domain," in *Proc. IEEE Int. Conf. Robot. Automat.*, May 2008, pp. 671–676.
- [16] J. W. Sensinger and S. Dosen, "A review of sensory feedback in upper-limb prostheses from the perspective of human motor control," *Front. Neurosci.*, vol. 14, Jun. 2020, Art. no. 345.
- [17] A. Iriki, M. Tanaka, and Y. Iwamura, "Coding of modified body schema during tool use by macaque postcentral neurones," *NeuroReport*, vol. 7, pp. 2325–2330, Oct. 1996.
- [18] A. Maravita and A. Iriki, "Tools for the body (schema)," *Trends Cogn. Sci.*, vol. 8, pp. 79–86, Feb. 2004.
- [19] M. Kawato, "Internal models for motor control and trajectory planning," *Curr. Opin. Neurobiol.*, vol. 9, pp. 718–727, Dec. 1999.
- [20] M. Yamagami, D. Howell, E. Roth, and S. A. Burden, "Contributions of feedforward and feedback control in a manual trajectory-tracking task," *IFAC-PapersOnLine*, vol. 51, pp. 61–66, Feb. 2019.
- [21] R. M. Robinson, D. R. R. Scobee, S. A. Burden, and S. S. Sastry, "Dynamic inverse models in human-cyber-physical systems," in *Proc. SPIE, Micro-Nanotechnol. Sensors Syst. Appl. VIII*, May 2016, Art. no. 98361X.

- [22] D. W. Franklin, R. Osu, E. Burdet, M. Kawato, and T. E. Milner, "Adaptation to stable and unstable dynamics achieved by combined impedance control and inverse dynamics model," *J. Neurophysiol.*, vol. 90, pp. 3270–3282, Nov. 2003.
- [23] E. Burdet, R. Osu, D. W. Franklin, T. E. Milner, and M. Kawato, "The central nervous system stabilizes unstable dynamics by learning optimal impedance," *Nature*, vol. 414, pp. 446–449, Nov. 2001.
- [24] I. Nisky, A. M. Okamura, and M. H. Hsieh, "Effects of robotic manipulators on movements of novices and surgeons," *Surg. Endoscopy*, vol. 28, pp. 2145–2158, Jul. 2014.
- [25] M. Singhal and J. D. Brown, "Telerobot operators can account for varying transmission dynamics in a visuo-haptic object tracking task," in *Proc. IEEE Int. Conf. Robot. Automat. (ICRA)*, May 2023, pp. 9814–9820.
- [26] R. W. Pew, "Human perceptual-motor performance," The Univ. Michigan, Ann Arbor, MI, Tech. Rep. 48, Aug. 1974.
- [27] W. Kim, F. Tendick, S. Ellis, and L. Stark, "A comparison of position and rate control for telemanipulations with consideration of manipulator system dynamics," *IEEE J. Robot. Autom.*, vol. RA-3, no. 5, pp. 426–436, Oct. 1987.
- [28] N. V. Dounskaia, S. P. Swinnen, C. B. Walter, A. J. Spaepen, and S. M. P. Verschueren, "Hierarchical control of different elbow-wrist coordination patterns," *Exp. Brain Res.*, vol. 121, pp. 239–254, Aug. 1998.
- [29] J. Mogk and P. Keir, "The effects of posture on forearm muscle loading during gripping," *Ergonomics*, vol. 46, pp. 956–975, Jul. 2003.
- [30] D. A. Forman, G. N. Forman, J. Robathan, and M. W. Holmes, "The influence of simultaneous handgrip and wrist force on forearm muscle activity," *J. Electromyogr. Kinesiol.*, vol. 45, pp. 53–60, Apr. 2019.
- [31] A. M. Zimmet, D. Cao, A. J. Bastian, and N. J. Cowan, "Cerebellar patients have intact feedback control that can be leveraged to improve reaching," *eLife*, vol. 9, Oct. 2020, Art. no. e53246.
- [32] C. S. Yang, N. J. Cowan, and A. M. Haith, "De novo learning versus adaptation of continuous control in a manual tracking task," *eLife*, vol. 10, Jun. 2021, Art. no. e62578.
- [33] R. C. Miall, G. Z. Reckess, and H. Imamizu, "The cerebellum coordinates eye and hand tracking movements," *Nature Neurosci.*, vol. 4, pp. 638–644, Jun. 2001.
- [34] R. Leib, A. Karniel, and F. A. Mussa-Ivaldi, "The mechanical representation of temporal delays," *Sci. Rep.*, vol. 7, Aug. 2017, Art. no. 7669.
- [35] E. Roth, K. Zhuang, S. A. Stamper, E. S. Fortune, and N. J. Cowan, "Stimulus predictability mediates a switch in locomotor smooth pursuit performance for *eigenmannia virescens*," *J. Exp. Biol.*, vol. 214, pp. 1170–1180, Apr. 2011.
- [36] M. Yamagami, L. N. Peterson, D. Howell, E. Roth, and S. A. Burden, "Effect of handedness on learned controllers and sensorimotor noise during trajectory-tracking," *IEEE Trans. Cybern.*, vol. 53, no. 4, pp. 2039–2050, Apr. 2023.



Jacob D. Carducci (Member, IEEE) received the B.S. in biomedical and mechanical engineering from the Rose-Hulman Institute of Technology, Terre Haute, IN, USA in 2016. He also received the M.S. degree in robotics and the Ph.D. degree in mechanical engineering from the Johns Hopkins University, Baltimore, MD, USA in 2018 and 2023 respectively. He is currently a Postdoctoral Researcher with the Danziger Laboratory, part of the Department of Rehabilitation Science, Emory University, Atlanta, GA, USA. His research focuses on how humans sense

environments and embody tools through physical interaction, how this haptic ability is impacted by neuro-physical changes, and how robotic tools can be built to identify and treat related diseases.



Noah J. Cowan (Fellow, IEEE) received the B.S. degree from the Ohio State University, Columbus, OH, USA in 1995, and the M.S. and Ph.D. degrees, in electrical engineering from the University of Michigan, Ann Arbor, MI, USA in 1997 and 2001 respectively. He was a Postdoctoral Fellow in integrative biology with the University of California, Berkeley, CA, USA for 2 years. In 2003, he joined the Mechanical Engineering department, Johns Hopkins University, Baltimore, MD, USA, where he is now a Professor. His research interests include mechanics and multi-sensory control in animals and machines. Prof. Cowan was the recipient of NSF PECASE award in 2010, the James S. McDonnell Foundation Scholar Award in Complex Systems in 2012, and two Johns Hopkins Discovery Awards in 2015, 2016, and 2023. In addition, Prof. Cowan received the William H. Huggins Award for excellence in teaching in 2004, and the Dunn Family Award in 2014, conferred for having "an extraordinarily positive impact upon the lives of one or more undergraduate students."



Jeremy D. Brown (Senior Member, IEEE) received the B.S., M.S., and Ph.D. degrees in mechanical engineering from the University of Michigan, Ann Arbor, MI, USA, in 2008, 2012, and 2014, respectively. He also received the B.S. degree in applied physics from Morehouse College, Atlanta, GA, USA. From 2014 to 2016, he completed a Postdoctoral Research Fellowship with the University of Pennsylvania, Philadelphia PA, USA. He is currently a John C. Malone Assistant Professor with the Department of Mechanical Engineering, Johns Hopkins University, Baltimore, MD, USA. His research focuses on the interface between humans and robots with a specific focus on medical applications and haptic feedback. He directs the Haptics and Medical Robotics Laboratory, which is part of the Laboratory for Computational Sensing and Robotics. Dr. Brown was the recipient of IEEE RAS Technical Committee on Haptics Early CAREER Award, the National Science Foundation CAREER Award, the Sloan Foundation Fellowship, the National Science Foundation CRII Award, the National Science Foundation Graduate Research Fellowship.